SAND2020-6524J

Turbulence/flame/wall interactions in non-premixed inclined slot-jet flames impinging at a wall using direct numerical simulation

Haiou Wang[a,*], Guo Chen[a], Kun Luo[a], Evatt R. Hawkes[b,c], Jacqueline H. Chen[d], Jianren Fan[a]

[a]*State Key Laboratory of Clean Energy Utilization, Zhejiang University, Hangzhou 310027, PR China*
[b]*School of Manufacturing and Mechanical Engineering, University of New South Wales, Sydney, NSW, 2052, Australia*
[c]*School of Photovoltaics and Renewable Energy Engineering, University of New South Wales, Sydney, NSW, 2052, Australia*
[d]*Sandia National Laboratories, Livermore, CA 94550, USA*

Abstract

In the present work, three-dimensional turbulent non-premixed oblique slot-jet flames impinging at a wall were investigated using direct numerical simulation (DNS). Two cases are considered with the Damköhler number (Da) of case A being twice that of case B. A 17 species and 73-step mechanism for methane combustion was employed in the simulations. It was found that flame extinction in case B is more prominent compared to case A. Reignition in the lower branch of combustion for case A occurs when the scalar dissipation rate relaxes, while no reignition occurs in the lower branch for case B due to excessive scalar dissipation rate. A method was proposed to identify the flame quenching edges of turbulent non-premixed flames in wall-bounded flows based on the intersections of mixture fraction and OH mass

*Corresponding author: Haiou Wang
Email address: wanghaiou@zju.edu.cn (Haiou Wang)

fraction iso-surfaces. The flame/wall interactions were examined in terms of the quenching distance and the wall heat flux along the quenching edges. There is essentially no flame/wall interaction in case B due to the extinction caused by excessive turbulent mixing. In contrast, significant interactions between flames and the wall are observed in case A. The quenching distance is found to be negatively correlated with wall heat flux as previously reported in turbulent premixed flames. The influence of chemical reactions and wall on flow topologies was identified. The FS/U and FC/U topologies are found near flame edges, and the NNN/U topology appears when reignition occurs. The vortex-dominant topologies, FC/U and FS/S, play an increasingly important role as the jet turbulence develops.
Keywords: Direct numerical simulation, Flame extinction, Flame/wall interaction, Flow topology

1. Introduction

Turbulence/flame/wall interactions in non-premixed flames are critical in many combustion systems including internal combustion engines, gas turbines and rocket engines [1]. In turbulent non-premixed flames, excessive turbulent mixing can result in extinction [2–5], which impacts fuel efficiency and pollutant emissions of the systems. Extinction phenomena have been studied extensively in turbulent non-premixed flames without walls experimentally [6] and numerically [2–5], and insights were gained into the physics involved. However, existing understanding of non-premixed flame extinction in wall-bounded flows is insufficient.

Flame/wall interactions have been studied in laminar and turbulent pre-

mixed flames [7–12]. Two generic interactions for premixed flames, *i.e.* head-on quenching (HOQ) and side-wall quenching (SWQ), were identified. Combustion is affected when bounded with walls, which might result in flame extinction; flames also have significant effects on quantities such as wall heat flux. Direct numerical simulation (DNS) of turbulent planar premixed flames propagating towards a wall was performed by Poinsot *et al.* [9], and negative correlations of the normalized wall heat flux and quenching distance were proposed. Turbulent V-shaped premixed flames in a channel were studied by Gruber *et al.* [12] and the statistics of wall heat flux were examined. Comparatively, there is much less effort regarding flame/wall interactions for non-premixed flames [13, 14], due to the fact that identifying the generic configurations is challenging [8, 15]. De Lataillade *et al.* [15] studied two-dimensional laminar non-premixed flames with strained HOQ. It was found that the quenching distance decreases while the corresponding wall heat flux increases with increasing strain. Turbulent non-premixed flames stabilized in the near-wall region were studied in [13], flame extinction due to wall cooling was discussed. The wall heat transfer of turbulent non-premixed wall-jet flames was discussed in [14]. Despite of the above studies, there has been no effort devoted to the interactions of flame quenching and wall heat flux for non-premixed flames in wall-bounded turbulent flows.

Combustion and wall also have considerable impacts on turbulence, which could be described by topological classifications [16]. Local flow topologies were studied in [17, 18] for non-premixed flames, and in [11, 19] for premixed flames. Lai *et al.* [11] studied flow topologies in turbulent V-shaped and planar premixed flames with a wall, and the effect of wall on flow topologies

was explored. It is of great interest to understand the interactions of flow topologies and wall-bounded combustion in non-premixed flame configurations.

In this work, interactions of turbulence, chemical reactions and the wall in non-premixed flames are explored. The contents of the paper are as follows. First, two turbulent non-premixed oblique slot-jet flames with different levels of extinction impinging at a wall are simulated using DNS. Second, the extinction behaviors of the two flames are described and the effects of turbulent mixing and wall on flame extinction are examined. Finally, the statistical results of flow toplologies, and the effects of chemical reactions and wall on flow topologies are presented and discussed.

2. Configuration and numerical methods

In the present work, a configuration of turbulent oblique slot-jet flames impinging at a flat wall is considered. The schematic of the configuration is shown in Fig. 1. The fuel jet consists of CH_4 and N_2, and is inclined to the wall with an angle of $\theta = 20^\circ$ to maximize the effect of flame/wall interactions. The geometry of oblique flames impinging at a flat wall has been commonly used in industrial and experimental configurations. For example, in the experiment of by Beér and Chigier [20], the flame was inclined to the wall with an angle of 20°. The oxidizer coflow is comprised of O_2 and N_2. Two cases with different fuel and oxidizer composition, case A and case B, are simulated. The composition of the fuel and oxidizer streams of the simulations is listed in Table 1. The composition was chosen so that the two cases feature different levels of extinction, as will be detailed shortly.

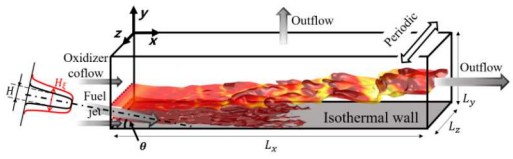

Figure 1: Schematic of the impinging slot-jet flame configuration.

The jet velocity, U_j, is 160 m/s, while the coflow velocity, U_c, is 40 m/s. The characteristic jet velocity, ΔU, is given by $U_j - U_c$. The profiles of mean velocity and mixture fraction at the inlet are based on hyperbolic tangent functions, which are described in the supplementary material. Here, the mixture fraction, ξ, is calculated based on the Bilger definition [21]. The jet width, H, is 1.1 mm and the width of the fuel slab, H_ξ, is 1.5 mm. The distance between the jet center and wall is $2H$ at the inlet. In the current study, H is smaller than H_ξ so that the jet could be developed before interacting with the flames. The jet Reynolds number, Re_j, based on ΔU and H, is 1910 for both cases.

The work focuses on turbulent non-premixed flames interacting with an isothermal wall with a temperature of $T_w = 573$ K. The radiative heat transfer was neglected to be more focused. The initial temperature for the jet is $T_j = 700$ K, and that for the coflow is $T_c = 573$ K, the same as T_w. The thermal conditions for the simulations are selected based on [22].

The simulations are initialized with laminar flamelet solutions using FlameMaster [23]. The initial scalar dissipation rate (χ) at the stoichiometric mixture fraction, χ_{st}, equals to $0.7\chi_q$ for both cases, where χ is the scalar dissipation rate defined as $\chi = 2D|\nabla\xi|^2$, and χ_q is the extinction scalar dissipation rate. D is the thermal diffusivity. For case A, χ_q is 2300 s^{-1}, and for case B, it

Table 1: Stream compositions of the simulations

	$\xi = 0$		$\xi = 1$	
	X_{O_2}	X_{N_2}	X_{CH_4}	X_{N_2}
Case A	0.4	0.6	0.8	0.2
Case B	0.34	0.66	0.8	0.2

is 1220 s^{-1}. Despite the turbulent flames are non-adiabatic, χ_q is estimated from adiabatic laminar flames for simplicity. The Damköhler number is defined as $Da = \chi_q t_j$, where t_j is the time scale defined as $t_j = H/\Delta U$. The Da values for case A and case B are 0.021 and 0.011, respectively, which are low enough to result in local extinction as will be shown in Sec. 3. The Da value for case A is about twice of that for case B; therefore, case A is expected to be more resilient to extinction than case B.

In order to trigger the jet turbulence, a turbulent velocity is superimposed at the inlet. The turbulence field is obtained by generating an auxiliary homogeneous isotropic turbulence based on an kinetic energy spectrum function by Passot-Pouquet [24]. The integral length scale of the turbulence field, l_t, equals to the jet width H and the turbulent velocity, u', is $0.1U_j$.

The computational domain is a rectangular box with $L_x \times L_y \times L_z = 42H \times 16H \times 8H$, where L_x, L_y and L_z are the domain length in the streamwise, x, wall-normal, y, and spanwise, z, directions, respectively. The boundary conditions are non-reflecting in the streamwise direction and periodic in the spanwise direction. No-slip isothermal wall ($y = 0$) and non-reflecting outflow ($y = L_y$) boundaries are used in the wall-normal direction. The grid resolution is uniform in the streamwise and spanwise and a stretch grid

profile is superimposed in the wall-normal direction to resolve properly the turbulence and flame scales. For turbulence, there is at least 0.6 grid for the Kolmogorov scale, η, in the whole domain. There are also more than 10 grids for solving flame structures. For both cases, the resultant grid number is $N_x \times N_y \times N_z = 1560 \times 560 \times 300$.

The DNS code S3D is used, which solves the Navier-Stokes equations for compressible reacting flows [25]. A six-stage fourth-order explicit Runge-Kutta method and an eighth-order central differencing scheme are employed for time integration and spatial derivatives [26], respectively. Fourth-order one-sided stencils are used at the boundaries of non-homogeneous directions. A tenth-order filter is used to remove high-frequency oscillations [26].

A 17 species and 73-step mechanism for methane combustion is employed in the DNS, among which 4 species (CH_2, CH_2(s), HCO and CH_2OH) are identified as quasi-steady state species. The mechanism is validated in steady counter-flow flames by comparing the results of various mechanisms, which is provided in the supplementary material. The simulations advanced for more than $3t_f$ after the flame achieved a statistically steady state to collect stationary statistics, where t_f is the flow-through time defined as $t_f = L_x/\Delta U$.

3. Results and discussion

In this section, the general characteristics of the impinging slot-jet flames are first examined and the flame extinction behaviors are reported. Then, the flame/wall interactions are investigated and the correlations between quenching distance and wall heat flux are revealed. Finally, the flow topologies conditioned on various regions of the flames are analyzed.

3.1. General characteristics

General results of the impinging slot-jet flames are presented. Fig. 2 shows the mean and instantaneous distributions of Y_{OH}, heat release rate and temperature for both cases. The dashed lines in the OH mass fraction plots indicate the location of the stoichiometric mixture fraction. The averages are performed in time and the homogeneous (spanwise) direction. Several observations can be made. First, converged statistics for various variables are obtained as reflected in the mean distributions. Second, flame extinction appears for both case A and case B. Here, flame extinction is identified as regions with low values of Y_{OH} and/or heat release rate along the stoichiometric mixture fraction iso-surface. Flame extinction is more prominent in case B compared to case A, which is consistent with the fact that Da for case B is lower than case A. Finally, the lower branch in case A is almost parallel to the wall over a long distance. Note that the dilatation effect from combustion modifies the trajectory of the stoichiometric mixture fraction iso-surface and pushes it upward. Therefore, the observed behaviour of the stoichiometric mixture fraction iso-surface is a competition between the mixing of the fuel and oxidizer streams and the dilation effect. The lower branch in case A is extinguished in the downstream region near the wall when the oxidizer is consumed completely. In contrast, the lower branch in case B is extinguished totally in the upstream region where there is still oxidizer available near the wall.

Figure 3 demonstrates the stoichiometric mixture fraction iso-surfaces colored by OH mass fraction and the three-dimensional volume rendering of vorticity magnitude for both cases. Extinction regions are highlighted

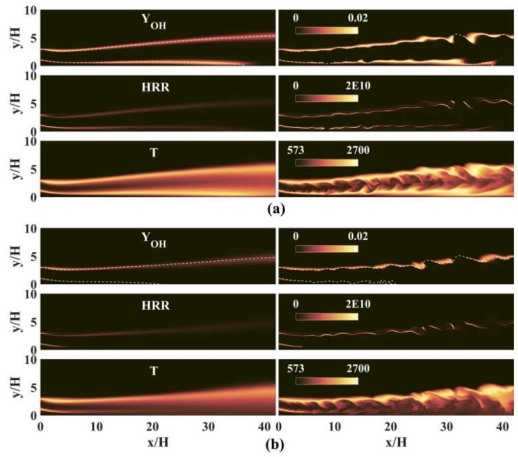

Figure 2: Mean (left) and instantaneous (right) distributions of OH mass fraction, heat release rate (J.m^{-3}.s^{-1}) and temperature (K) for (a) case A and (b) case B. The dashed lines in the OH mass fraction plots indicate the location of the stoichiometric mixture fraction.

in black. To define the extinction regions, we first assume that extinction occurs on stoichiometric mixture fraction iso-surfaces, corresponding to high heat release rate. A region along these iso-surfaces is considered extinction if Y_{OH} is lower than 10% of its maximum value, $Y_{OH,max}$, in the entire domain. The sensitivity of the results to the choice of the threshold is provided in the supplementary material. A similar definition of flame extinction has been employed by Pantano [4] for identifying flame edges.

The two branches for each case are clearly observed in Fig. 3. As can be seen, the extinction behaviors are different for the two branches and between the two cases. For case A, few extinction regions are identified for the upper branch in the downstream region ($x/H > 25$); extinction is observed for the lower branch in the upstream region ($x/H < 5$) and in the downstream region where the oxidizer is completely consumed. As for case B, extinction

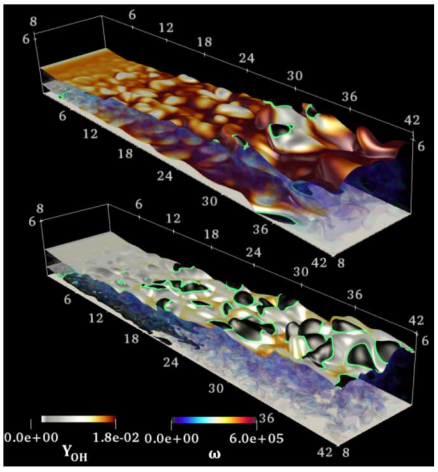

Figure 3: Stoichiometric mixture fraction iso-surface colored by OH mass fraction and three-dimensional volume rendering of vorticity magnitude for case A (top) and case B (bottom). The extinction region is illustrated in black.

frequently occurs on the upper branch after $x/H = 10$; the lower branch is totally extinguished after $x/H = 5$. The visualization also indicates that there is a strong correlation between the extinction regions and the surface curvature. Particularly, the center of the extinction regions tends to be in the fuel side. This observation is consistent with Lignell *et al.* [3] for turbulent non-premixed jet flames without a wall.

More quantitative analyses of flame extinction are provided. Fig. 4a shows the statistical results of burning fraction on the stoichiometric mixture fraction iso-surfaces conditioned on various regions. The burning fraction is defined as the ratio of the burning area to the total area on the stoichiometric mixture fraction iso-surfaces. It is seen that the extinction of the upper branch for case A is not obvious, consistent with Fig. 3. Evident extinction is observed for the upper branch of case B, and the minimum burning fraction

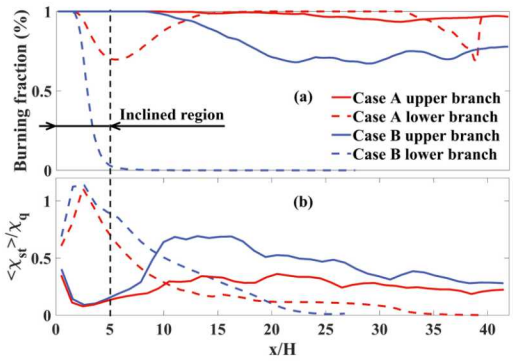

Figure 4: Evolution of (a) burning fraction and (b) normalized scalar dissipation rate on the stoichiometric mixture fraction iso-surface.

appears around $x/H = 20 \sim 30$. For the oblique slot-jet flame configuration, an inclined region based on the mean flow field is identified from $x/H = 0$ to 5. In the inclined region, the burning fraction decreases for the lower branch with increasing axial distance for both cases. The burning fraction is minimum at $x/H = 5$ for case A, after which reignition occurs and the burning fraction is increased until extinction due to the depletion of oxygen. However, the flame is totally extinguished for the lower branch of case B after $x/H = 5$, and the burning fraction vanishes.

The statistics of scalar dissipation rate on stoichiometric mixture fraction iso-surfaces conditioned on various regions are shown in Fig. 4b. The scalar dissipation rate for case A and case B is normalized by their respective extinction scalar dissipation rate (χ_q). It can be seen that, for the upper branch, the scalar dissipation rate first decreases in the inclined region due to the relaxation of the flow for both cases; then it increases and reaches a maximum around $x/H = 15$; finally, the scalar dissipation rate decreases in the downstream region due to turbulence relaxation. It is also seen that the

normalized scalar dissipation rate is well below unity for the upper branch of both cases. The scenario is different for the low branch. Particularly, the normalized scalar dissipation rate first increases in the inclined region and its maximum value is larger than unity for both cases. Reignition occurs for case A after $x/H = 5$ when the scalar dissipation rate relaxes. In contrast, the peak of the scalar dissipation rate for case B is so high that the entire branch is extinguished and no reignition occurs.

3.2. Flame/wall interactions

From the perspective of practical applications, one of the most important quantities is wall heat flux, Φ. The wall heat flux is defined as $\Phi = -\lambda \partial T/\partial y$, where λ is the thermal conductivity. The evolution of mean wall heat flux along the streamwise direction is presented in Fig. 5. As can be seen, the wall heat flux first increases with increasing downstream distance for case A before reaching its peak around $x/H = 36$; then the wall heat flux decreases further downstream. It is noted that the peak wall heat flux corresponds to the wall extinction region. On the other hand, the wall heat flux increases monotonically with increasing downstream distance for case B, and plateaus after $x/H = 25$. The magnitude of wall heat flux in case B is also considerably lower than case A. This is due to the total extinction of the lower branch for case B as shown in Figs. 3 and 4.

Flame/wall interactions can be described by two variables, *i.e.* the distance between the quenching edge and the wall, δ_q, and the corresponding wall heat flux, Φ_q. The quenching Peclet number, P_q, is defined as the quenching distance normalized by the premixed flame thickness δ_L, *i.e.* $P_q = \delta_q/\delta_L$, and the normalized wall heat flux, ϕ_q, is defined as $\phi_q =$

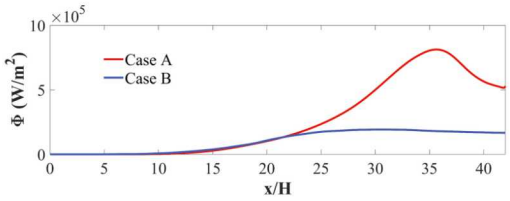

Figure 5: Evolution of mean wall heat flux for case A and case B.

$\Phi_q/(\rho_u s_l c_p(T_2 - T_1))$, where ρ_u is the reactant density, s_l is the laminar flame velocity, c_p is the specific heat capacity, and T_2 and T_1 are the temperature of the products and reactants, respectively. The reference values for normalization are from a corresponding laminar stoichiometric premixed flame, which has also been widely used in previous studies [9, 12]. It is noted that flame propagation plays an important role in flame edges [5, 27], which justifies the use of reference values from premixed flames in the present work. A schematic of the quenching edge is illustrated in Fig. 6a, which is obtained by extracting the intersections of the stoichiometric mixture fraction surface and the Y_{OH} iso-surface with $Y_{OH} = 0.1 \times Y_{OH,max}$. The instantaneous distributions of wall heat flux for case A and case B are shown in Fig. 6b and Fig. 6c, respectively. The projection of quenching edges on the wall is also superimposed, which is colored by quenching Peclet numbers. As mentioned earlier, the total extinction of the lower branch for case B occurs in the upstream region and far way from the wall. Therefore, the corresponding quenching Peclet numbers are large and wall heat flux is small. There is essentially no flame/wall interaction for this case. In contrast, the quenching Peclet numbers are small in the downstream regions of case A, and significant flame/wall interactions are observed, where the oxygen is consumed completely and the flame extinguishes. Note that for the local extinction that occurs in the up-

stream regions of case A, the values of P_q are large and the wall heat flux is small, which is not considered in the analysis of flame/wall interactions.

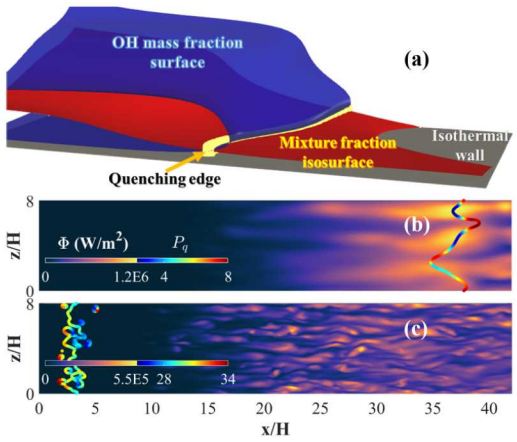

Figure 6: Schematic of (a) the quenching edge. Instantaneous distributions of wall heat flux for (b) case A and (c) case B where the projection of quenching edges colored by quenching Peclet numbers is also superimposed.

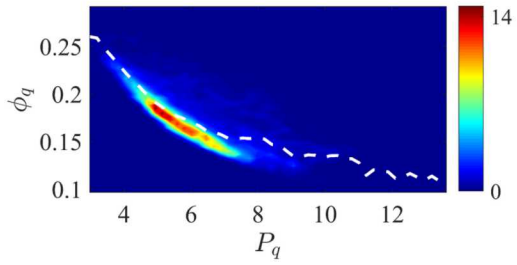

Figure 7: The joint PDF of the normalized wall heat flux and quenching distance for case A.

The joint PDF of P_q and ϕ_q for case A is demonstrated in Fig. 7, where the white dashed line indicates the conditional mean of ϕ_q. The joint PDF is calculated as $f(P_q, \phi_q) = \partial^2 F(P_q, \phi_q)/\partial P_q \partial \phi_q$, where $F(P_q, \phi_q)$ is the cumulative distribution function. It is obvious that the quenching distance

and wall heat flux are negatively correlated. The most probable normalized quenching distance is about 5.0 and the corresponding normalized wall heat flux is 0.18. It is also interesting to see that the correlations between P_q and ϕ_q are close to those in previous studies of premixed flames [9].

3.3. Flow topology

In the presence of turbulent oblique slot-jet flames impinging at the wall, turbulence is inevitably influenced by chemistry and wall. In order to have a better understanding of local flow structures in wall-bounded flames, flow topologies conditioned on various regions are explored. The local flow topologies are characterized by the velocity gradient tensor $A_{ij} = \partial u_i/\partial x_j = S_{ij} + W_{ij}$, where $S_{ij} = (A_{ij} + A_{ji})/2$ is the strain rate tensor and $W_{ij} = (A_{ij} - A_{ji})/2$ is the rotation tensor. The eigenvalues of the velocity gradient tensor are λ_1, λ_2 and λ_3, which are the solutions of the characteristic equation $\lambda^3+P\lambda^2+Q\lambda+R = 0$ with the invariants specified as $P = -S_{ii}$, $Q = (P^2 - S_{ij}S_{ji} - W_{ij}W_{ji})/2$ and $R = (-P^3+3PQ - S_{ij}S_{jk}S_{ki} - 3W_{ij}W_{jk}S_{ki})/3$. For compressible flows, 27 possible topological classifications could be identified in the PQR space [16]. Consistent with several previous DNS studies of flow topologies [17–19], only a subset of the classifications are observed in the present work. The flow topologies and their descriptions are provided in Table 2, which can be categorized as strain-dominant nodal regions (S2, S3, S6 and S8) and vortex-dominant foci regions (S1, S4, S5 and S7). A schematic of these flow topologies is shown in the supplementary material.

Figure 8 illustrates sequential distributions of flow topologies and heat release rate in a typical $x-y$ region of case A. The gray dashed and red solid lines indicate stoichiometric mixture fraction and $Y_{OH} = 0.1 \times Y_{OH,max}$ iso-

Table 2: Classification of flow topology types

	Acronym	Description
S1	FC/U	Foci/Compressing, Unstable
S2	NSS/U	Node/Saddle/Saddle, Unstable
S3	NSS/S	Node/Saddle/Saddle, Stable
S4	FS/S	Foci/Stretching, Stable
S5	FC/S	Foci/Comprssing, Stable
S6	NNN/S	Node/Node/Node, Stable
S7	FS/U	Foci/Stretching, Unstable
S8	NNN/U	Node/Node/Node, Unstable

lines, respectively. Iso-lines of heat release rate and vorticity magnitude are superimposed on Fig. 8a and iso-lines of scalar dissipation rate are superimposed on Fig. 8b. It can be seen that vortical structures with high vorticity magnitude in the shear layer are dominant by the FS/S topology, which are surrounded by the FC/U and NSS/U topologies. This is consistence with previous DNS of Grout *et al.* [17] for a jet in cross-flow configuration. There are two edge flames and a flame hole identified in Fig. 8. The evolutions of the edge flames and flame hole are revealed in the time sequences. Particularly, high scalar dissipation rate is observed at $t = 276.5\tau_j$ near the edge flames, which is largely responsible for the formation of flame hole [2, 4, 5]. The scalar dissipation rate relaxes in flame regions at $t = 282.5\tau_j$ and the flame hole tends to reignite. Detailed analyses of edge flame dynamics are beyond the scope of this work and here we focus on the interactions of flow topologies and flames. As can be seen in Fig. 8, there is a region with high

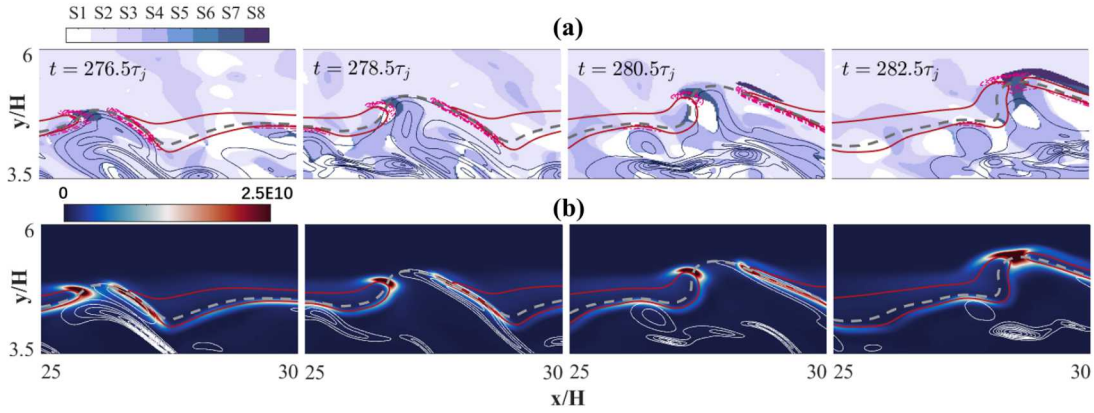

Figure 8: Sequential images of (a) flow topological classifications superimposed with heat release rate (magenta dash-dotted lines) and vorticity magnitude (black solid lines) and (b) heat release rate superimposed with scalar dissipation rate (white solid lines) for the upper branch of case A from $x/H = 25$ to 30. The gray dashed and red solid lines indicate stoichiometric mixture fraction and $Y_{OH} = 0.1 \times Y_{OH,max}$ iso-lines, respectively.

heat release rate near the flame edge of the left branch, which is characterized by the FS/U and FC/U topolologies. At $t = 280.5$ and $282.5\tau_j$ when reignition occurs, the FS/U and NNN/U topologies appear in the vicinity of flame edges with significant heat release rates. The local positive dilatation (negative P), which caused by heat release, plays a significant role in determining the flow topology distribution[28]. The first invariant P also affects the second and third invariants (Q and R), and these invariants determine the local flow topologies. Similar observations have been made previously. For example, Grout *et al.* [17] and Cifuentes *et al.* [19] found the FS/U and NNN/U topologies in regions with enhanced chemical reactions.

In order to highlight the effects of chemistry on flow topologies, the statistics from both burning and extinction regions are examined in various regions. Fig. 9 shows the volume fractions of flow topologies of case A and

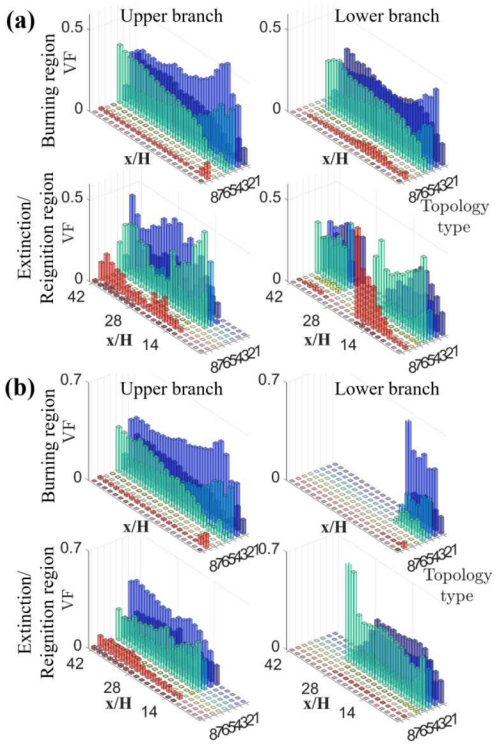

Figure 9: The volume fractions of flow topologies of case A and case B conditioned on various regions.

case B conditioned on the vicinity of stoichiometric mixture fraction, *i.e.* $\xi_{st} - 0.0015 \leq \xi \leq \xi_{st} + 0.0015$. As can be seen, the strain-dominant topologies, *i.e.* NSS/U and NSS/S dominate the near field for both cases. As the jet turbulence develops in the downstream region, the vortex-dominant topologies of FC/U and FS/S play an increasingly important role. It is also seen that the FS/U and NNN/U topologies are rarely observed in burning regions but they occur in extinction/reignition regions, which is related to the large positive dilatation due to heat release at flame edges as discussed in Fig. 8. The occurrence of the FS/U and NNN/U topologies could, there-

fore, be a potential indicator of the extinction/reignition event in the present configuration. The effects of wall on flow topologies are obvious in extinction/reignition regions of the lower branch of case A with the volume fraction of FS/U being decreased when wall quenching occurs due to reduced heat release.

4. Conclusions

A DNS study of turbulent non-premixed oblique slot-jet flames impinging at a flat wall has been presented. Two cases are considered. The Da value of case A is twice that of case B. The interactions of turbulence, chemical reactions and the wall are explored. The main findings are summarized as follows. *First*, flame extinction is more evident in case B than case A. The lower branch of case B is totally extinguished due to excessive turbulent mixing, and no reignition occurs. *Second*, significant flame/wall interactions are found in case A, where the quenching Peclet numbers are negatively correlated with the normalized wall heat flux. There is essentially no interaction of flames and the wall in case B. *Finally*, the turbulence structures are considerably affected by chemical reactions. The FS/U and NNN/U topologies are rarely observed in burning regions but they occur in extinction/reignition regions with significant heat release rates. As the shear-generated turbulence develops, the volume fractions of the vortex-dominant topologies of FC/U and FS/S increases consistently.

Acknowledgments

This work was supported by Natural Science Foundation of China (Grant No.: 51836007, 51976185) and the Fundamental Research Funds for the Central Universities. The work at Sandia National Laboratories was supported by the US Department of Energy, Office of Basic Energy Sciences, Division of Chemical Sciences, Geosciences, and Biosciences. Sandia National Laboratories is a multimission laboratory managed and operated by National Technology and Engineering Solutions of Sandia, LLC., a wholly owned subsidiary of Honeywell International, Inc., for the U.S. Department of Energys National Nuclear Security Administration under contract DE-NA- 0003525.

References

[1] A. Dreizler, B. Böhm. Advanced laser diagnostics for an improved understanding of premixed flame-wall interactions. Proc. Combust. Inst. 35 (2015) 37–64.

[2] E. R. Hawkes, R. Sankaran, J. C. Sutherland, J. H. Chen. Scalar mixing in direct numerical simulations of temporally evolving plane jet flames with skeletal CO/H_2 kinetics. Proc. Combust. Inst. 31 I (2007) 1633–1640.

[3] D. O. Lignell, J. H. Chen, H. A. Schmutz. Effects of Damköhler number on flame extinction and reignition in turbulent non-premixed flames using DNS. Combust. Flame 158 (2011) 949–963.

[4] C. Pantano. Direct simulation of non-premixed flame extinction in a

methane-air jet with reduced chemistry. J. Fluid Mech. 514 (2004) 231–270.

[5] S. Karami, E. R. Hawkes, M. Talei, J. H. Chen. Mechanisms of flame stabilisation at low lifted height in a turbulent lifted slot-jet flame. J. Fluid Mech. 777 (2015) 633–689.

[6] S. Kaiser, J. Frank. Spatial scales of extinction and dissipation in the near field of non-premixed turbulent jet flames. Proc. Combust. Inst. 32 (2009) 1639–1646.

[7] P. Popp, M. Baum. Analysis of wall heat fluxes, reaction mechanisms, and unburnt hydrocarbons during the head-on quenching of a laminar methane flame. Combust. Flame 108 (1997) 327–348.

[8] F. Dabireau, B. Cuenot, O. Vermorel, T. Poinsot. Interaction of flames of $H_2 + O_2$ with inert walls. Combust. Flame 135 (2003) 123–133.

[9] T. J. Poinsot, D. C. Haworth, G. Bruneaux. Direct simulation and modeling of flame-wall interaction for premixed turbulent combustion. Combust. Flame 95 (1993) 118–132.

[10] G. Bruneaux, K. Akselvoll, T. Poinsot, J. H. Ferziger. Flame-wall interaction simulation in a turbulent channel flow. Combust. Flame 107 (1996) 27–36.

[11] J. Lai, N. Chakraborty, P. Zhang, L. Wang. Heat flux and flow topology statistics in oblique and head-on quenching of turbulent premixed flames by isothermal inert walls. Combust. Sci. Tech. 191 (2019) 353–381.

[12] A. Gruber, R. Sankaran, E. R. Hawkes, J. H. Chen. Turbulent flame-wall interaction: A direct numerical simulation study. J. Fluid Mech. 658 (2010) 5–32.

[13] Y. Wang, A. Trouvé. Direct numerical simulation of nonpremixed flame–wall interactions. Combust. Flame 144 (2006) 461–475.

[14] Z. Pouransari, L. Vervisch, L. Fuchs, A. V. Johansson. DNS analysis of wall heat transfer and combustion regimes in a turbulent non-premixed wall-jet flame. Flow Turbul. Combust. 97 (2016) 951–969.

[15] A. De Lataillade, F. Dabireau, B. Cuenot, T. Poinsot. Flame/wall interaction and maximum wall heat fluxes in diffusion burners. Proc. Combust. Inst. 29 (2002) 775–779.

[16] M. S. Chong, A. E. Perry, B. J. Cantwell. A general classification of three-dimensional flow fields. Phys. Fluids A 2 (1990) 765–777.

[17] R. W. Grout, A. Gruber, C. S. Yoo, J. H. Chen. Direct numerical simulation of flame stabilization downstream of a transverse fuel jet in cross-flow. Proc. Combust. Inst. 33 (2011) 1629–1637.

[18] W. Han, A. Scholtissek, F. Dietzsch, R. Jahanbakhshi, C. Hasse. Influence of flow topology and scalar structure on flame-tangential diffusion in turbulent non-premixed combustion. Combust. Flame 206 (2019) 21–36.

[19] L. Cifuentes, C. Dopazo, J. Martin, C. Jimenez. Local flow topologies and scalar structures in a turbulent premixed flame. Phys. Fluids 26 (2014) 065108.

[20] J. M. Beér, N. A. Chigier. Impinging jet flames. Combust. Flame 12 (1968) 575–586.

[21] R. W. Bilger. The structure of diffusion flames. Combust. Sci. Tech. 13 (1976) 155–170.

[22] A. Montanaro, L. Allocca, G. Meccariello, M. Lazzaro. Schlieren and mie scattering imaging system to evaluate liquid and vapor contours of a gasoline spray impacting on a heated wall. SAE Tech. Pap. 2015 (2015) 10.

[23] H. Pitsch, M. Bollig. FlameMaster v3. 3.10, A C++ computer program for 0d combustion and 1d laminar flame calculations (2015) .

[24] T. Passot, A. Pouquet. Numerical simulation of compressible homogeneous flows in the turbulent regime. J. Fluid Mech. 181 (1987) 441–466.

[25] J. H. Chen, A. Choudhary, B. De Supinski, M. Devries, E. R. Hawkes, S. Klasky, W. K. Liao, K. L. Ma, J. Mellor-Crummey, N. Podhorszki, R. Sankaran, S. Shende, C. S. Yoo. Terascale direct numerical simulations of turbulent combustion using S3D. Comput. Sci. Disc. 2 (2009) 015001.

[26] C. A. Kennedy, M. H. Carpenter. Several new numerical methods for compressible shear-layer simulations. Appl. Numer. Math. 14 (1994) 397–433.

[27] G. R. Ruetsch, L. Vervisch, A. Lin. Effects of heat release on triple flames. Phys. Fluids 7 (1995) 1447–1454.

[28] J. Lai, D. H. Wacks, N. Chakraborty. Flow topology distribution in head-on quenching of turbulent premixed flame: A direct numerical simulation analysis. Fuel 224 (2018) 186–209.